A New Active Damping Control Strategy for LCL Converter in Hybrid Coordinate System

Meng Jia
Power Electronics Institute
Beijing Jiaotong University
Beijing, China
17121447@bjtu.edu.cn

Fei Lin
Power Electronics Institute
Beijing Jiaotong University
Beijing, China
flin@bjtu.edu.cn

Sai Wang
Yangtze River Delta Research Institute
Beijing Jiaotong University
Beijing, China
11121675@bjtu.edu.cn

Zhongping Yang
Power Electronics Institute
Beijing Jiaotong University
Beijing, China
zhpyang@bjtu.edu.cn

Xiao Deng
Power Electronics Institute
Beijing Jiaotong University
Beijing, China
17121420@bjtu.edu.cn

***Abstract*—Compared with L filter, LCL filter is favored because of its advantages of volume and low cost. LCL filter suffers from resonance problem. In this paper, the active damping strategy using only grid current is further studied. Firstly, it is pointed out that the reason for the resonance problem is the absence of the characteristic equation corresponding to the transfer function of the output current i_g to the input voltage u_{inv}. The model analysis of LCL part proves that the system is strongly coupled in *dq* synchronous rotating frame, and the highest coupling term is second differential term, which makes decoupling difficult. Then the active damping strategy in hybrid coordinate system is proposed. The closed-loop control of dc-link voltage and grid-connected current is finished in *dq* synchronous rotating frame and the active damping control strategy is finished in *αβ* stationary frame. In the discrete *z*-domain, the root locus method is used to design the parameters of the controller and the active damper, and the effectiveness of the proposed strategy is proved by using MATLAB/Simulink.**

Keywords—LCL filter, active damping, resonance suppression

I. INTRODUCTION

With the rapid development of China's economy and urbanization, urban rail transit develops rapidly. Urban rail transit has the advantages of high speed, large volume and high comfort. It can effectively solve the problem of road congestion and travel difficulty in big cities by using Metro or light rail. For the sake of energy saving, the Metro energy feedback device will become the main way of regenerative braking energy feedback for rail transit vehicles in the future. Metro energy feedback device not only has the function of inverting feedback, but also has the functions of traction rectification and reactive power compensation. As the mainstream topology, three-phase four-quadrant converter topology selection, filter optimization design and control have become the focus of current scholars in various countries.

Three-phase four-quadrant converters mostly adopt current control mode. When pulse width modulation (PWM) is adopted, a large number of current high frequency harmonics will be generated. In order to suppress these high frequency harmonics, L filter or LCL filter are traditionally used [1]. Compared with L filter, the total inductance required by LCL filter is relatively smaller, so the size of the filter is smaller and the cost is lower [2],[14]. The advantages of LCL filter are remarkable in high power applications such as wind power system and energy feedback devices.

LCL filter is a third-order system, and its gain is attenuated at - 60dB slope in high frequency band [3]. It can reduce ripple at switching frequency and suppress high-order harmonics of current effectively. However, one of the difficulties in the control of LCL converter is its resonance problem. Its frequency response has a resonance peak at the resonance frequency, which shows a very large gain. At the same time, the phase will jump, so the resonance peak needs to be damped to stabilize the system. Passive damping method is simple to implement, but it will cause additional losses [4]-[6], which is not allowed in the case of high efficiency requirements. Active damping has become a hot research topic.

In active damping strategies, additional sensors are needed in [7]-[14]. It uses the measured capacitance branch current as feedback variable in [7]-[10] and the purpose is to parallel virtual resistors in capacitor branch, so as to achieve the equivalent of passive damping method. References [11]-[13] use the measured capacitance voltage as feedback variable. The weighted average current control is used in [14]. These control strategies increase additional hardware costs, and because of the increase of variables, the control algorithm is relatively complex and the robustness of the system is reduced.

In order to avoid additional sensing, it is proposed in the [15] that the system can be stable without damping when satisfying $\omega_{res}>\omega_s/6$. The reason is that the transport delays in digital control will introduce an inherent damping. Under weak power grid and the introduction of digital control will reduce the equivalent ω_{res} of the system, which will lead to the instability of the system. References [16]-[20] only need to modify the algorithm to achieve active damping. An active damping strategy based on high-pass filter (HPF) is adopted in [17]-[18],[20], which can achieve active damping only by measuring grid currents, and the design of parameters is relatively simple. Because the control is completed in *abc*/*αβ* frame, the reactive power can not be controlled easily. It adopts the same strategy to control in *dq* frame in [17], but does not consider the complex current decoupling relationship and the robustness of the system.

Based on the above research and in-depth analysis of LCL filter model, this paper proposes an active damping strategy based on HPF in hybrid coordinate system in Section II and Section III. To achieve a stable system, a systematic co-design

978-1-7281-2124-6/19/$31.00

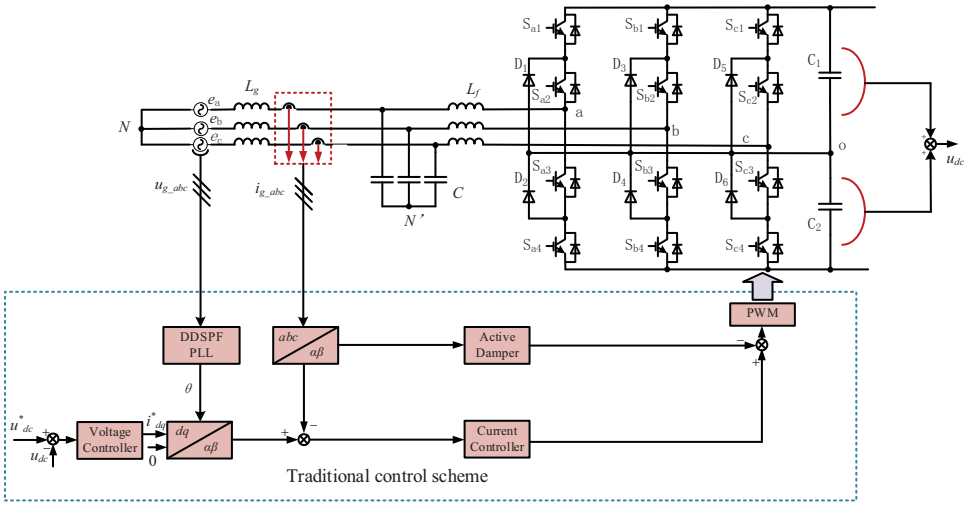

Fig.1 Traditional control strategy of three-phase four-quadrant converter based on HPF

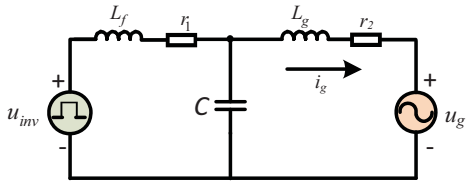

Fig.2 Single-phase equivalent circuit based on LCL filter

procedure for the active damping and grid current controller is introduced in Section IV. Finally, the proposed strategy is verified through Matlab/Simulink in Section V and Section VI is the conclusion. It should be noted that this paper focuses on the control of the inner current loop in detail, and does not make additional analysis of the outer dc-link voltage loop.

II. LCL Filter Model Analysis

A. System Description

The main circuit of three-level four-quadrant converter and its active damping control block diagram are shown in Fig.1. LCL filter is used as the filter. L_g is the grid side inductance; L_f is the converter side inductance; r_1 and r_2 represent the stray inductance of the line. Assuming that the three-phase parameters are identical, the single-phase equivalent circuit is obtained as shown in Fig. 2.

In the actual circuit, the stray inductance of each part is usually small. The analysis below ignores the spurious parameters, and the LCL filter has no damping, which means it works in the worst environment. In order to prevent the influence of harmonics in the point of common coupling (PCC) on the control system, the decoupled double synchronous reference frame phase-locked loop (DDSPF-PLL) is adopted. This kind of phase-locked loop (PLL) can accurately lock the phase in the harsh environment of the power grid, thereby improving the control accuracy.

In the equivalent circuit shown in Fig. 2, according to the circuit principle, the relationship between grid side current i_g and converter side voltage u_{inv} is obtained as follows:

$$G_{lcl}(s)=\frac{i_g(s)}{u_{inv}(s)}=\frac{1}{L_fL_gCs^3+(L_f+L_g)s} \tag{1}$$

From the (1), it can be seen that the resonance of LCL filter is due to the absence of s^2 term in the characteristic equation of its transfer function. Therefore, the essence of the damping method is to introduce appropriate s^2 term to make the system no longer resonant.

B. Modeling of LCL Filter

The LCL part of the converter shown in Fig. 1 is modeled in *abc* stationary frame, and the following equation is obtained:

$$\begin{aligned}\left[v_{inv\_i}\right]&=\left[v_{c\_i}\right]+L_f p\left[i_{f\_i}\right]\\ \left[v_{c\_i}\right]&=\left[v_{g\_i}\right]+L_g p\left[i_{g\_i}\right]-v_{NN'}[1,1,1]^T\\ \left[i_{f\_i}\right]&=\left[i_{g\_i}\right]+Cp\left[v_{c\_i}\right]\end{aligned} \tag{2}$$

where $[v_{inv\_i}]=[v_{inv\_a}, v_{inv\_b}, v_{inv\_c}]^T$ represents the three-phase converter side voltage, $[v_{c\_i}]=[v_{c\_a}, v_{c\_b}, v_{c\_c}]^T$ represents the voltage of three-phase filter capacitor, $[v_{g\_i}]=[v_{g\_a}, v_{g\_b}, v_{g\_c}]^T$ represents the three-phase voltage of the PCC , $[i_{f\_i}]=[i_{f\_a}, i_{f\_b}, i_{f\_c}]^T$ represents the three-phase converter side current, $[i_{g\_i}]=[i_{g\_a}, i_{g\_b}, i_{g\_c}]^T$ represents the three-phase grid side current, $p=d/dt$ represents the differential operator and $v_{NN'}$ represents the voltage from the common point N of the grid side to the common point N' of the filter capacitor.

The above (2) can be transformed into $\alpha\beta$ stationary frame, and the transformation and its inverse transformation used in this paper are defined by:

$$\begin{aligned}\left[x_{\_\alpha\beta}\right]&=[\mathrm{C}]\left[x_{\_\mathrm{abc}}\right],[\mathrm{C}]=\frac{2}{3}\begin{bmatrix}1 & -1/2 & -1/2\\ 0 & \sqrt{3}/2 & -\sqrt{3}/2\end{bmatrix}\\ \left[x_{\_abc}\right]&=\frac{3}{2}[\mathrm{C}]^T\left[x_{\_\alpha\beta}\right],[\mathrm{C}]^T=\frac{2}{3}\begin{bmatrix}1 & 0\\ -1/2 & \sqrt{3}/2\\ -1/2 & -\sqrt{3}/2\end{bmatrix}\end{aligned} \tag{3}$$

where $[x\_\alpha\beta]=[x\_\alpha, x\_\beta]^T$, x represents the voltages or currents.

Applying (3) to transform (2), and the mathematical model in the $\alpha\beta$ stationary frame is obtained as follows:

$$\begin{aligned}\left[v_{inv\_\alpha\beta}\right]&=\left[v_{c\_\alpha\beta}\right]+L_f p\left[i_{f\_\alpha\beta}\right]\\ \left[v_{c\_\alpha\beta}\right]&=\left[v_{g\_\alpha\beta}\right]+L_g p\left[i_{g\_\alpha\beta}\right]\\ \left[i_{f\_\alpha\beta}\right]&=\left[i_{g\_\alpha\beta}\right]+Cp\left[v_{c\_\alpha\beta}\right]\end{aligned} \tag{4}$$

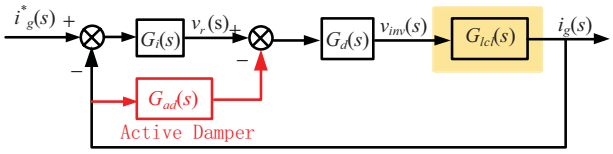

(a)

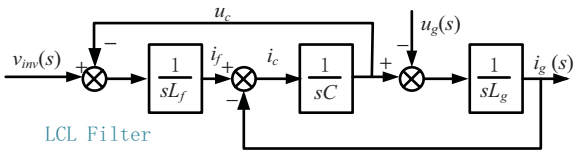

(b)

Fig.3 Active damping control block diagram based on HPF

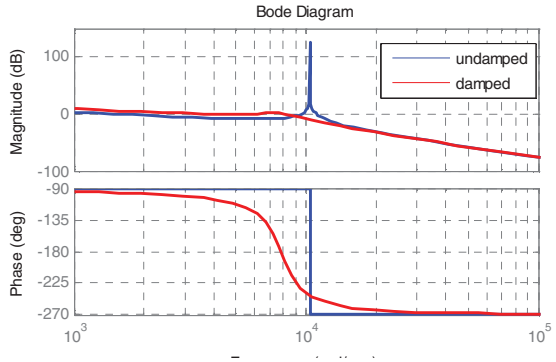

Fig.4 Bode diagrams of systems before and after damping

where $[v_{inv\_\alpha\beta}]=[v_{inv\_\alpha}, v_{inv\_\beta}]^T$ represents the voltage value of the converter side in the $\alpha\beta$ frame, $[v_{c\_\alpha\beta}]=[v_{c\_\alpha}, v_{c\_\beta}]^T$ represents the voltage value of the filter capacitor in the $\alpha\beta$ frame, $[v_{g\_\alpha\beta}]=[v_{g\_\alpha}, v_{g\_\beta}]^T$ represents the voltage value of the grid side in the $\alpha\beta$ frame, $[i_{f\_\alpha\beta}]=[i_{f\_\alpha}, i_{f\_\beta}]^T$ represents the converter side current in the $\alpha\beta$ frame, $[i_{g\_\alpha\beta}]=[i_{g\_\alpha}, i_{g\_\beta}]^T$ represents the current value of the grid side in the $\alpha\beta$ frame.

Further, by combining the three equations in (4), it is obtained that the relationship between the voltage $v_{inv\_\alpha\beta}$ of the converter side and the current $i_{g\_\alpha\beta}$ of the grid side is as follows:

$$\left[v_{inv\_\alpha\beta}\right]=\left[v_{g\_\alpha\beta}\right]+(L_f+L_g)p\left[i_{g\_\alpha\beta}\right]+L_fCp^2\left[v_{c\_\alpha\beta}\right] \quad (5)$$

From the mathematical model of *abc* stationary frame and $\alpha\beta$ stationary frame, the *abc* three phases or $\alpha\beta$ two phases are independent of each other, so many literatures adopted *abc* three-phase control or $\alpha\beta$ two-phase control separately. In addition, it can be seen from (5) that the voltage $v_{inv\_\alpha\beta}$ is related not only to the voltage and current on the grid side, but also to the secondary differential of the capacitive voltage.

The following transformation and its inverse transformation are defined as:

$$\begin{aligned}\left[x_{\_dq}\right]&=[G]\left[x_{\_\alpha\beta}\right],[G]=\begin{bmatrix}\cos\omega t & \sin\omega t\\ -\sin\omega t & \cos\omega t\end{bmatrix}\\ \left[x_{\_dq}\right]&=[G]^{-1}\left[x_{\_dq}\right],[G]^{-1}=\begin{bmatrix}\cos\omega t & -\sin\omega t\\ \sin\omega t & \cos\omega t\end{bmatrix}\end{aligned} \quad (6)$$

where $[x\_dq]=[x\_d, x\_q]^T$, x represents the voltages or currents.

Applying (6) to transform (4), and the mathematical model in the *dq* synchronous rotating frame is obtained as follows:

$$\begin{aligned}\left[v_{inv\_dq}\right]&=\left[v_{c\_dq}\right]+L_f[\mathrm{T}]\left[i_{f\_dq}\right]\\ \left[v_{c\_dq}\right]&=\left[v_{g\_dq}\right]+L_g[\mathrm{T}]\left[i_{g\_dq}\right]\\ \left[i_{f\_dq}\right]&=\left[i_{g\_dq}\right]+C[\mathrm{T}]\left[v_{c\_dq}\right]\end{aligned} \quad (7)$$

$$[\mathrm{T}]=\begin{bmatrix}p & -\omega\\ \omega & p\end{bmatrix}$$

where $[v_{inv\_dq}]=[v_{inv\_d}, v_{inv\_q}]^T$ represents the voltage value of the converter side in the *dq* frame, $[v_{c\_dq}]=[v_{c\_d}, v_{c\_q}]^T$ represents the voltage value of the filter capacitor in the *dq* frame, $[v_{g\_dq}]=[v_{g\_d}, v_{g\_q}]^T$ represents the voltage value of the grid side in the *dq* frame, $[i_{f\_dq}]=[i_{f\_d}, i_{f\_q}]^T$ represents the converter side current in the *dq* frame, $[i_{g\_dq}]=[i_{g\_d}, i_{g\_q}]^T$ represents the current value of the grid side in the *dq* frame, T represents coupling matrix.

By combining the three equations in (7), it is obtained that the relationship between the voltage v_{inv_dq} of the converter side and the current i_{g_dq} of the grid side is as follows:

$$\left[v_{inv\_dq}\right]=[\mathrm{A}]\left[v_{g\_dq}\right]+[\mathrm{B}]\left[i_{g\_dq}\right] \quad (8)$$

where $[A]=E+L_fCT^2$, E is a unit array;

$$[B]=(L_f+L_g)T+L_fL_gCT^3$$

From the above (8), it can be seen that the three-phase converter based on LCL filter is a strong coupling system in *dq* synchronous rotating frame.

III. Active Damping Strategy in Hybrid Frame

Reference [18] proposes a control strategy for active damping only by measuring the grid side current. The block diagram is shown in Fig. 3, and the active damper is:

$$G_{ad}(\mathrm{s})=-k_d\frac{s}{s+\omega_{ad}} \quad (9)$$

In the (9), k_d is the coefficient of active damper and ω_{ad} is the cut-off frequency of HPF. An additional gain of '$-k_d$' is added after HPF to ensure that the active damper generates an additional 180° phase compensation at the resonant frequency.

After introducing G_{ad} term in the control scheme,

$$\frac{i_g(\mathrm{s})}{u_{inv}(\mathrm{s})-G_{ad}(\mathrm{s})i_g(\mathrm{s})}=\frac{1}{L_fL_gCs^3+(L_f+L_g)s} \quad (10)$$

By transforming the (10), the transfer function of the damped system can be obtained in (11) shown at the top of next page.

Compared with (1), an additional s^2 item is added, but due to the introduction of G_{ad}, an open-loop zero point is added. Fig. 4 shows the Bode diagram before and after adding the damper.

From Fig.4, we can see that the resonance peaks are obviously suppressed by introducing G_{ad}. At the same time, it can be seen that the introduction of damper does not affect the

$$G_{lcl\_damped}(s)=\frac{i_g(s)}{u_{inv}(s)}=\frac{s+\omega_{ad}}{L_fL_gCs^4+L_fL_gC\omega_{ad}s^3+(L_f+L_g)s^2+(L_f\omega_{ad}+L_g\omega_{ad}-k_d)s} \tag{11}$$

$$[B]=\begin{bmatrix} L_fL_gCp^3+(L_f+L_g-3L_fL_gC\omega^2)p & -3L_fL_gC\omega p^2+L_fL_gC\omega^3-(L_f+L_g)\omega \\ 3L_fL_gC\omega p^2-L_fL_gC\omega^3+(L_f+L_g)\omega & L_fL_gCp^3+(L_f+L_g-3L_fL_gC\omega^2)p \end{bmatrix}$$

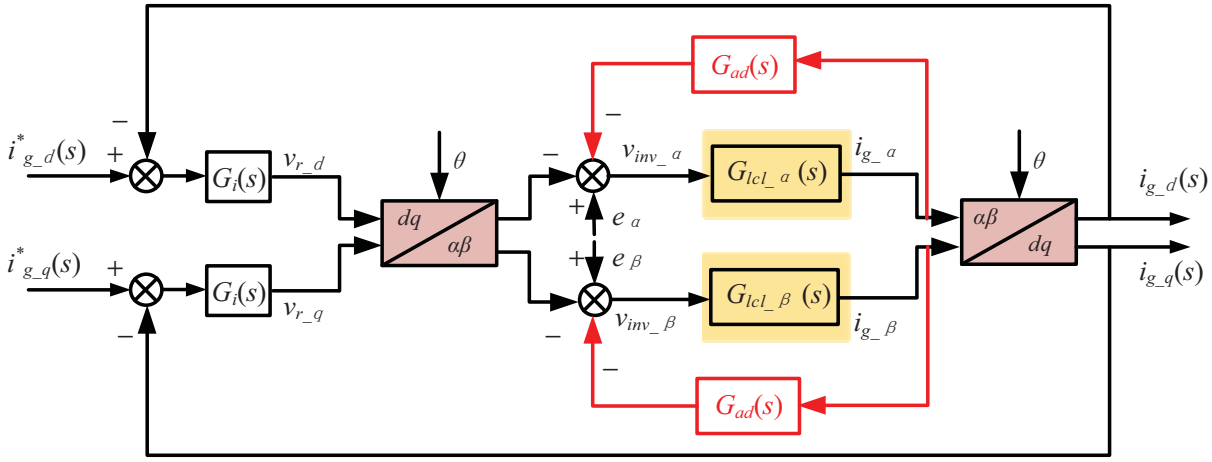

Fig.5 Active damping strategy based on HPF in hybrid coordinate system considering current loop only

attenuation of high frequency band, but the gain of low frequency band increases slightly.

The $G_d(s)$ in Fig. 3 represents the delay of digital control, which is composed by the half sampling period introduced by PWM delay and one sampling period of computation delay, and it can be expressed as follows:

$$G_d(s)=e^{-1.5T_s s} \tag{12}$$

Current loop control is adopted in *abc* frame or *αβ* frame in [18],[20]. In order to eliminate the static error of current control, PR controller is needed as current controller, whose transfer function is as follows:

$$G_i(s)=k_p+\frac{2k_r\omega_i s}{s^2+2\omega_i s+\omega_o^2} \tag{13}$$

where k_p is the proportional coefficient of the controller, k_r is the resonant coefficient, ω_i is the bandwidth of the resonant term considering the requirement of -3dB, and ω_0 is the fundamental angular frequency.

Although this method can achieve precise control of grid side current, it can not accurately control active and reactive power components of the system. In addition, when using digital control, the PR controller is more complex than PI controller.

Reference [17] completes the control in *dq* synchronous rotating frame, because of the existence of active loop and reactive loop, it is easy to control the active power and reactive power of the converter. PI controller is used as the current controller. Its transfer function is as follows:

$$G_i(s)=k_p+\frac{k_i}{s} \tag{14}$$

where k_p is the proportional coefficient of the controller and k_i is the integral coefficient.

From (8) deduced above, it can be seen that the i_d and i_q loops are strongly coupled in the *dq* synchronous rotating frame. In order to achieve accurate control of the grid side current, the following conditions need to be added to the control scheme:

1) Considering the feedforward matrix [A] of grid voltage and [A] is as follows:

$$[A]=\begin{bmatrix} 1+L_fC(p^2-\omega^2) & -2L_fC\omega p \\ 2L_fC\omega p & 1+L_fC(p^2-\omega^2) \end{bmatrix}$$

where p represents differential operator, corresponding to the 's' in complex frequency domain.

p^2 appears in the principal diagonal of the matrix, that is to say, the secondary differential of e_d and e_q is needed. For the control system, the differential usually amplifies the noise. Therefore, it is difficult to realize the decoupling when considering the feed-forward matrix of grid voltage.

2) Considering the matrix [B], the current loop is decoupled. The expression is shown at the top of the page.

From the expression, it can be seen that the highest coupling term is second differential term, and the coupling is strong. Therefore, it is difficult to decouple.

Considering the above strategies, an active damping control strategy in hybrid coordinate system is proposed. As shown in Fig. 5, the closed-loop control of dc-link voltage and grid-connected current is finished in *dq* frame and the active damping control strategy is finished in *αβ* frame. The proposed strategy has the following advantages:

1) The active damping control part is independent, without complex decoupling function, and it only need to add the unit grid voltage feed-forward compensation.

2) It can directly control the active and reactive components of the grid-connected current of the converter.

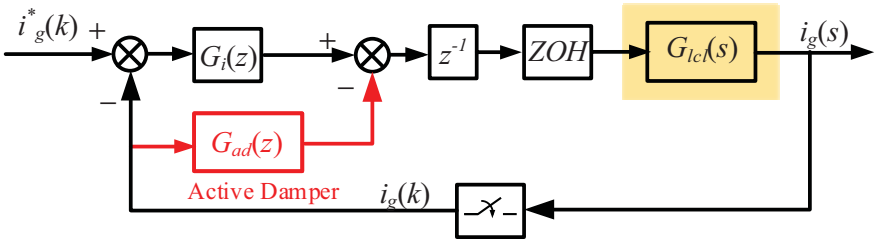

Fig.6 Active damping strategy in discrete z-domain

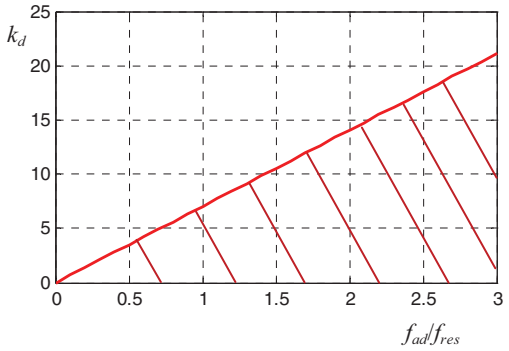

Fig.7 The relationship between k_d and ω_{ad}

TABLE I. THE SYSTEM PARAMETERS

Symbol	*Electrical Constant*	*value*
P	Rated power	50kW
u_{dc}	DC-link voltage	600V
u_g	Grid voltage	210V
f_0	Grid frequency	50Hz
f_{sw}	Switching frequency	5kHz
f_s	Sampling frequency	5kHz
L_f	Converter-side inductor	0.55mH
L_g	Grid side inductor	0.126mH
C	Filter capacitor	90μF

3) A simpler PI controller can be used for both dc-link voltage and grid current control, which is easy to realize.

IV. STABILITY ANALYSIS AND PARAMETER DESIGN IN DISCRETE Z-DOMAIN

For the whole system, the analysis of LCL filter model is continuous, and it is more accurate in the *s*-domain. For the control part, considering the problem of delay caused by digital control, the analysis of the whole system in the discrete *z*-domain is closer to the actual system. In this section, the parameters of the control system are designed based on the stability analysis in *z*-domain. The parameters of the system are shown in Table.I.

A. System Model in z-domain

Fig.6 shows the control block diagram in the discrete *z*-domain. The computation delay of digital control is represented by z^{-1}. ZOH represents zero-order holder and the expression is as follows:

$$G_{zoh}(s)=\frac{1-e^{-sT_s}}{s} \tag{15}$$

The ZOH and the transfer function of LCL filter are transformed by the equation in (16) and the result is shown in (17)

$$z=e^{sT_s} \tag{16}$$

$$\begin{aligned} G_{z\_lcl}(z) &= Z\left[G_{zoh}(s)*G_{lcl}(s)\right] \\ &= \frac{T_s}{(L_f+L_g)(z-1)} \\ &\quad -\frac{\sin(\omega_{res}T_s)(z-1)}{\omega_{res}(L_f+L_g)[z^2-2z\cos(\omega_{res}T_s)+1]} \end{aligned} \tag{17}$$

where ω_{res} represents the resonant frequency of LCL filters and is determined by the following formula:

$$\omega_{res}=\sqrt{\frac{L_f+L_g}{L_fL_gC}} \tag{18}$$

For the current controller, PI controller is adopted in this paper. Considering that current closed-loop control and active damping strategy are accomplished in different frames, it points out that PI controller in *dq* frame is equivalent to PR controller in *αβ* frame [9]. When using PR controller, resonance coefficient k_r is introduced to reduce steady-state error of current. For stability analysis , the proportional gain k_p can be considered only, but the PI controller is still used in practice. The expression of the discrete *z*-domain of PI controller after backward differential transformation is as follows:

$$G_i(z)=k_p+k_i\frac{T_sz}{z-1} \tag{19}$$

After the active damper is discretized, the expression is as follows:

$$G_{ad}(z)=-k_d\frac{z-1}{(\omega_{ad}T_s+1)z-1} \tag{20}$$

By using (17)-(20), the open-loop gain $G_{op}(z)$ and closed-loop gain $G_{cl}(z)$ of the whole current loop can be obtained respectively as follows:

$$G_{op}(z)=\frac{z^{-1}G_i(z)G_{z\_lcl}(z)}{1+z^{-1}G_{ad}(z)\,G_{z\_lcl}(z)} \tag{21}$$

$$G_{cl}(z)=\frac{z^{-1}G_i(z)G_{z\_lcl}(z)}{1+z^{-1}[G_{ad}(z)+G_i(z)]G_{z\_lcl}(z)} \tag{22}$$

B. Parameter Design in z-domain

Based on the main circuit parameters listed in the Table.I, the following steps are adopted to design the current controller parameters k_p, k_i and k_d, ω_{ad} in active damper.

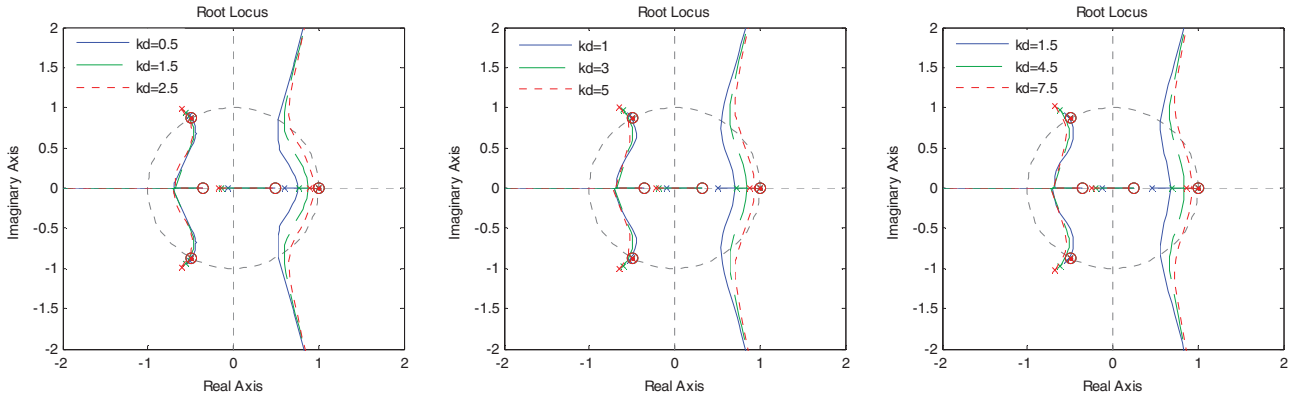

(a) (b) (c)

Fig.8 The root locus diagrams with different values of ω_{ad}. (a) ω_{ad} =0.5ω_{res}. (b) ω_{ad} =ω_{res}. (c) ω_{ad} =1.5ω_{res}.

TABLE II. THE CONTROL PARAMETERS

Symbol	***Electrical Constant***	***value***
k_p	proportional coefficient	1.062
k_i	integral coefficient	314
f_{ad}	Cutoff frequency of HPF	2484
k_d	Coefficient of active damper	0.8

Step1: The upper limit of k_d for a given parameter. According to Routh's criterion, the stability of the current loop is based on the fact that all the order parameters of the denominator part s of (11) are positive. Therefore, the following expression can be obtained:

$$k_d \le (L_f + L_g)\omega_{ad} = 2\pi(L_f + L_g) f_{ad} \tag{23}$$

We can see from the (23) that the upper limit of k_d is affected by ω_{ad}, so the range of k_d needs to be further determined. Meanwhile, in order to explore the relationship between k_d and ω_{ad}, Fig.7 is obtained. The red curve in Fig.7 is the upper limit of k_d, and the shadow part is the area where k_d changes with f_{ad}.

Step2: The design of current controller parameters k_p and k_i. The parameters k_p and k_i of current controller are designed by traditional design method in this paper. In order to reduce the influence of negative phase shift of PI controller on phase margin, the loop gain at cutoff frequency f_{co} should be guaranteed to be 1. Considering the effects of ZOH and digital control beat lag , the design is as follows [17]:

$$\begin{aligned} k_p &= \pi f_{co}(L_f + L_g) \\ k_i &= \frac{k_p}{10\pi(L_f + L_g)} \end{aligned} \tag{24}$$

For cutoff frequency f_{co}, it is necessary to keep away from resonance frequency f_{res} as far as possible so as not to cause instability by introducing -180° phase lag. Considering comprehensively, f_{co} needs to satisfy the following expression [21]:

$$f_{co} \approx 0.3 f_{res} \tag{25}$$

Step3: Parameter design of k_d and ω_{ad}. As we can see from (23), the two parameters are interacting . In this paper, we first design ω_{ad} and then design k_d.

The value of ω_{ad} should not be too high because it is the cut-off frequency of extracting high-frequency components, which will inevitably mix part of the noise. This paper chooses ω_{ad} satisfies:

$$\omega_{ad} \le 1.5\omega_{res} < 0.5\omega_s \tag{26}$$

The corresponding k_d satisfies:

$$k_d \le 1.5(L_f + L_g)\omega_{res} \tag{27}$$

The subsequent root locus plots in Fig.8 are for three different cutoff frequencies of HPF (ω_{ad} = 0.5ω_{res} , ω_{res} , 1.5ω_{res}) and for each frequency, three k_d values are chosen uniformly in the upper limit. The root locus diagram only considers the continuous change of k_p.

It can be seen from Fig. 8 that after selecting ω_{ad}, with the increase of k_d, the two root loci in the right half plane of the graph approach to the unit circle, and the value of k_p in the stable region of the unit circle shrinks continuously, that is, the system tends to be unstable gradually. Therefore, the value of k_d near the boundary should be avoided. Meanwhile, with the increase of k_d, the two root loci in the left half plane of the graph gradually extend out of the unit circle, which means that the system gain k_p is in the range of 0 to a certain boundary value, and the closed-loop poles of the system are also outside the unit circle. If the k_p parameter designed is less than the boundary value, the system will also be unstable. In fact, for the root locus analysis of a set of given parameters, the range of k_p parameters that make the system stable can be read directly from the graph by using the commands of Matlab. For example, when ω_{ad} = 1.5ω_{ad} and k_d = 1.5 are selected, the range of k_p that makes the system stable is (0.5413, 2.9228). The design parameter of k_p is 1.062 in this paper, and k_d can be adjusted again.

V. SIMULATION VERIFICATION

In order to verify the proposed active damping control strategy in hybrid coordinate system, a simulation model is built by MATLAB/Simulink. The parameters of the simulation model are shown in Table I. The parameters of the control section are shown in Table II.

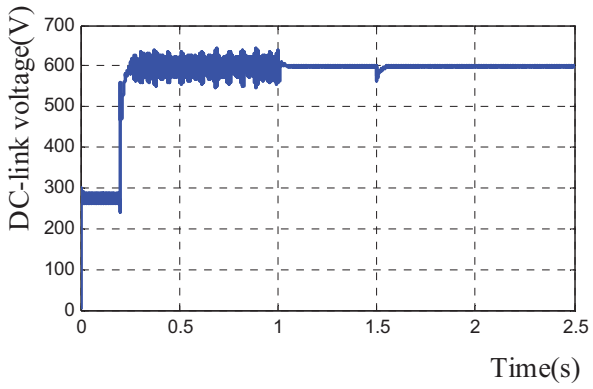

(a)

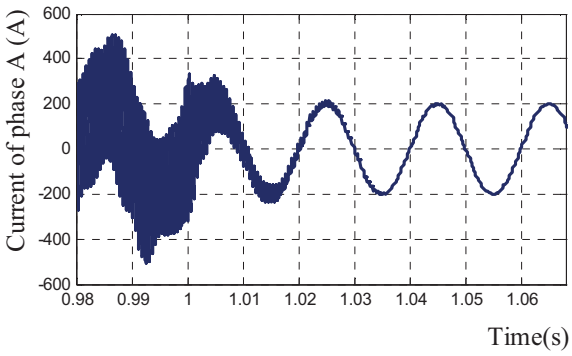

(b)

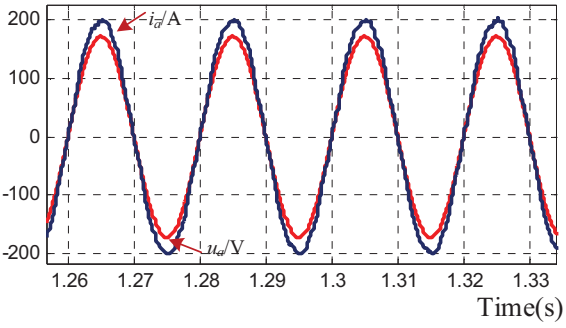

(c)

Fig.9 Simulation results with proposed strategy.(a) DC-link voltage. (b) current of phase A.(c) AC voltage and current of phase A

In the simulation, besides the current inner loop, there is a voltage outer loop to stabilize the dc-link voltage, and the load is a resistive load. The simulation waveforms of the active damping control strategy in hybrid coordinate system proposed in this paper are shown in Fig 9 and the simulation waveforms of the active damping control strategy only in the *dq* frame are shown in Fig 10. When t = 0.2s, the pulse is enable in the simulation experiment. When t = 1s, the active damper is introduced.

We can be seen from Fig 9(b) that after the introduction of active damper, the AC current gradually stabilizes from resonance state to no longer resonance, which proves the effectiveness of active damper. In steady state, the dc voltage

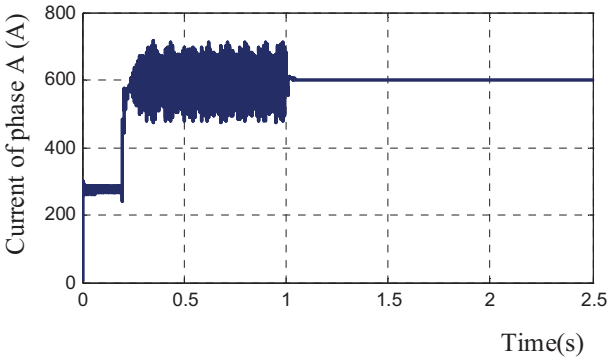

(a)

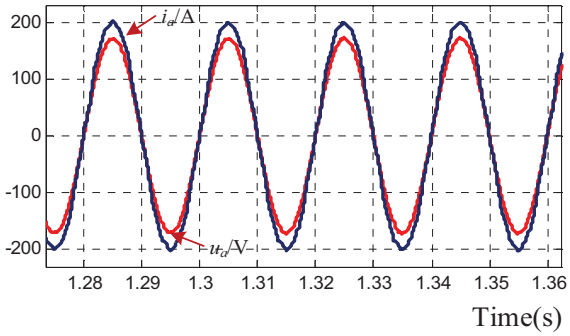

(b)

Fig.10 Simulation results with the strategy only in the dq frame. (a) DC-link voltage. (b) AC voltage and current of phase A.

reaches the rated 600V shown in Fig.9(a) and the current reaches the rated amplitude 200A shown in Fig.9(b). Through FFT analysis of Simulink, the fundamental amplitude of the current is 199.9A and THD is 2.85%, which meets the IEEE Std 929-2000. It can be seen from Fig.9(c) that the voltage and current on the grid side are basically in the same frequency and the same phase. The magnification observation shows that the phase differences between grid voltage and grid current is close to the strategy only in the *dq* frame shown as Fig10(b), which means the effect is not obvious. This is because when the control in *dq* frame is adopted, for the decoupling matrix [B], if ω is small, then the system will satisfy:

$$|3L_fL_gC\omega p^2 - L_fL_gC\omega^3| \ll |(L_f + L_g)\omega|$$

$$|L_fL_gCp^3 - 3L_fL_gC\omega^2 p| \ll (L_f + L_g)p$$

[B] can be approximately reduced to

$$[B] \approx \begin{bmatrix} (L_f + L_g)p & -(L_f + L_g)\omega \\ (L_f + L_g)\omega & (L_f + L_g)p \end{bmatrix}$$

Similarly, [A] can be approximately reduced to

$$[A] \approx \begin{bmatrix} 1 & 0 \\ 0 & 1 \end{bmatrix}$$

Therefore, there is little difference between the two strategies. Obviously, the proposed strategy achieves more precise current control than the control strategy only in *dq* frame.

In order to verify the dynamic response performance of the system, 20% load is added suddenly when t = 1.5s. It can be seen from Fig.9(a) that the dynamic response of the system is fast and no overshoot, which means the system is good.

VI. Conclusion

This paper is a further study of active damping strategy for only measuring grid current. Aiming at the characteristics of control in $\alpha\beta$ stationary frame and dq synchronous rotating frame, an active damping control strategy in hybrid coordinate system is proposed. Compared with control in $\alpha\beta$ stationary frame, this new strategy only needs a relatively simple PI controller instead of PR controller. Compared with control in dq synchronous rotating frame, the precise control of current can be achieved without considering the complex decoupling relationship. Based on the proposed control strategy, the parameters of controller and active damper are designed and their stability in discrete z-domain is analyzed. The simulation results show that the control strategy is feasible and the dynamic response of the system is good.

Acknowledgment

This work is supported by Beijing Jiaotong University.

References

[1] F. Blaabjerg, R. Teodorescu, M. Liserre, and A. Timbus, “Overview of control and grid synchronization for distributed power generation systems,” IEEE Trans. Ind. Electron, vol. 53, no. 5, pp. 1398–1409, Oct. 2006.

[2] S. Mariethoz and M. Morari, "Explicit Model-Predictive Control of a PWM Inverter With an LCL Filter," in IEEE Transactions on Industrial Electronics, vol. 56, no. 2, pp. 389-399, Feb. 2009.

[3] J. Dannehl, M. Liserr, and F. W. Fuchs, “Filter-based active damping of voltage source converters with LCL filter,” IEEE Trans. Ind. Electron., vol. 58, no. 8, pp. 3623–3633, Aug. 2011.

[4] Pena-Alzola R, Liserre M, Blaabjerg F, Sebastian R, Dannehl J, Fuchs FW. “Analysis of the passive damping losses in lcl-filter-based grid converters,” IEEE Trans Power Electron, 2013,28:2642–6.

[5] Zhang C, Dragicevic T, Vasquez JC, Guerrero JM. “Resonance damping techniques for grid-connected voltage source converters with LCL filters – a review,” IEEE Int Energy Conf ,2014:169–76.

[6] Beres R, Wang X, Blaabjerg F, Bak CL, Liserre M. “A review of passive filters for grid-connected voltage source converters,” In Proceedings of the IEEE appl. Power electron. conf. expo, 2014. p. 2208–15.

[7] F. Liu, Y. Zhou, S. Duan, J. Yin, B. Liu, and F. Liu, “Parameter design of a two-current-loop controller used in a grid-connected inverter system withLCL filter,” IEEE Trans. Ind. Electron, vol. 56, no. 11, pp. 4483–4491, Nov. 2009.

[8] W. Gullvik, L. Norum, and R. Nilsen, “Active damping of resonanceoscillations in LCL-filters based on virtual flux and virtual resistor,” in Proc. Eur. Conf. Power Electron. Appl, 2007, pp. 1–10.

[9] E. Twining and D. G. Holmes, “Grid current regulation of a three-phasevoltage source inverter with an LCL input filter,” IEEE Trans. Power Electron, vol. 18, no. 3, pp. 888–895, May 2003.

[10] X. Wang, X. Ruan, S. Liu, and C. K. Tse, “Full feedforward of grid voltage for grid-connected inverter with LCL filter to suppress current distortion due to grid voltage harmonics,” IEEE Trans. Power Electron, vol. 25, no. 12, pp. 3119–3126, Dec. 2010

[11] K. Jalili and S. Bernet, “Design of LCL filters of active-front-end two level voltage-source converters,” IEEE Trans. Ind. Electron, vol. 56, no. 5, pp. 1674–1689, May 2009.

[12] J. L. Agorreta, M. Borrega, J. López, and L. Marroyo, “Modeling and control of N-paralleled grid-connected inverters with LCL filter coupled due to grid impedance in PV plants,” IEEE Trans. Power Electron, vol. 26, no. 3, pp. 770–785, Mar. 2011.

[13] M. H. Bierhoff and F. W. Fuchs, “Active damping for three-phase PWM rectifiers with high-order line-side filters,” IEEE Trans. Ind. Electron, vol. 56, no. 2, pp. 371–379, Feb. 2009.

[14] G. Shen and D. Xu, “An improved control strategy for grid-connectedvoltage source inverters with an LCL filter,” IEEE Trans. Power Electron, vol. 23, no. 4, pp. 1899–1906, Jul. 2008

[15] J. Yin, S. Duan, and B. Liu, “Stability analysis of grid-connected inverter with LCL filter adopting a digital single-loop controller with inherent damping characteristic,” IEEE Trans. Ind. Informat, vol. 9, no. 2, pp. 1104–1112, May 2013

[16] C. Dick, S. Richter, M. Rosekeit, J. Rolink, and R. De Doncker, “Activedamping of LCL resonance with minimum sensor effort by means of a digital infinite impulse response filter,” in Proc. Eur. Conf. Power Electron, 2007, pp. 1–8.

[17] M. Hanif, V. Khadkikar, W. Xiao, and J. L. Kirtley, “Two degrees of freedom active damping technique for LCL filter based grid connected PV systems,” IEEE Trans. Ind. Electron, vol. 61, no. 6, pp. 2795–2803, Jun. 2014.

[18] J. Xu, S. Xie, and T. Tang, “Active damping-based control for grid connected LCL-filtered inverter with injected grid current feedback only,” IEEE Trans. Ind. Electron, vol. 61, no. 9, pp. 4746–4758, Sep. 2014.

[19] B. Bahrani, M. Vasiladiotis, and A. Rufer, “High-order vector control of grid-connected voltage-source converters with LCL-filters,” IEEE Trans. Ind. Electron, vol. 61, no. 6, pp. 2767–2775, Jun. 2014

[20] Wang X, Blaabjerg F, Loh PC. “Grid-current-feedback active damping for LCLresonance in grid-connected voltage-source converter,” IEEE Trans Power Electron, vol. 31, no. 1, pp. 213–223, Jan. 2016.

[21] Y. Tang, P. C. Loh, P. Wang, F. H. Choo, F. Gao, and F. Blaabjerg,“Generalized design of high performance shunt active power filter without put LCL filter,” IEEE Trans. Ind. Electron, vol. 59, no. 3, pp. 1443–1452, Mar. 2012.